Pergamon

0022-3697(96)00293-6

J. Phys. Chem Solids Vol 57, No. 5, pp. 571–587, 1996
Copyright © 1996 Elsevier Science Ltd
Printed in Great Britain. All rights reserved
0022-3697/96 $15.00 + 0.00

POLARIZED ELECTRONIC SPECTRA OF THE $(CH_3NH_3)_2Cd_{1-x}Mn_xCl_4$ ($x = 0$–1) PEROVSKITE LAYER DOPED WITH Cu^{2+}: STUDY OF THE $Cl^- \rightarrow Cu^{2+}$ CHARGE TRANSFER INTENSITY ENHANCEMENT ALONG THE SERIES

RAFAEL VALIENTE and FERNANDO RODRIGUEZ
DCITIMAC, Facultad de Ciencias, Universidad de Cantabria, 39005 Santander, Spain

(*Received* 6 *July* 1995; *accepted in revised form* 25 *September* 1995)

Abstract—The polarized optical absorption spectra of the 2-D $A_2Cd_{1-x}Mn_xCl_4$ ($x = 0$–1; A = CH_3NH_3) crystals doped with Cu^{2+} are investigated. The analysis of both the charge transfer and crystal field spectra indicates that the copper impurities form $CuCl_6^{4-}$ complexes with an elongated D_{2h} (nearly D_{4h}) symmetry. A salient feature is the enhancement of charge transfer band intensity as well as the presence of new intense bands at 21000 and 25000 cm^{-1} observed on passing from $x = 0$ to $x = 1$ along the series. These bands are associated with Mn–Cu aggregates whose superexchange pathways involve the short (equatorial) Cu–Cl bond (25000 cm^{-1}) and the long (axial) Cu–Cl bond (21000 cm^{-1}) of the $CuCl_6^{4-}$ complex. A noteworthy fact of these exchange coupled Mn–Cu systems is that the transition energy of the first Mn^{2+} excitations are resonant with the $Cl^- \rightarrow Cu^{2+}$ charge transfer transitions. This effect seems to play a fundamental role in the enhancement of intensity. The temperature dependence of the oscillator strength allowed us to estimate a ground state exchange constant $J \approx 70\,cm^{-1}$ for the Mn–Cu pair. The results are compared with those obtained in Mn–Cu aggregates in fluorides.

Keywords: $CuCl_6^{4-}$, exchange coupled Mn–Cu systems, charge transfer spectra, $(RNH_3)_2Cd_{1-x}Mn_xCl_4$ crystals, spectroscopic and structural correlations

1. INTRODUCTION

The optical properties of Jahn–Teller (JT) Cu^{2+} have been intensively investigated due to its single electronic configuration (d^9) and the variety of coordination geometries displayed mainly by heteroligand Cu^{2+} complexes or even by CuX_n complexes (X = F, Cl or Br; $n = 4$ or 6) formed in different inorganic compounds. In general, the charge transfer (CT) and crystal field (CF) electronic spectra strongly depend on the nature of the ligands, X, the coordination number, n, and the local geometry around the Cu^{2+}, i.e., Cu–X distances and coordination symmetry [1]. When Cu^{2+} replaces a divalent cation, the occurrence of a given geometrical structure for CuX_n depends on the complex itself as well as on the host crystal. The knowledge of such a structure is actually a difficult task to be accomplished *a priori* [2, 3]. The bending distorted tetrahedral (D_{2d}) and the elongated octahedral (D_{4h}) geometries usually found for CuX_4^{2-} and CuX_6^{4-} complexes, respectively, can be significantly modified by crystal anisotropy or interactions with neighboring atoms, this latter situation being particularly important when hydrogen bonds are involved. The *compressed* octahedral (D_{4h}) symmetry found for CuF_6^{4-} in $KCuAlF_6 : Cu^{2+}$ [4], $Ba_2ZnF_6 : Cu^{2+}$ [5] and $K_2ZnF_4 : Cu^{2+}$ [6, 7] and the square planar (D_{4h}) symmetry found for $CuCl_4^{2-}$ complexes formed in $(creatinium)_2CuCl_4$ and $(nmph)_2CuCl_4$ [3, 8] are examples of this behavior. Interestingly, there are several Cu^{2+} doped or pure materials for which the occurrence of structural phase transitions (SPT) induced either by temperature or pressure, can be accompanied by abrupt changes in the local structure around Cu^{2+} that can lead to an intense thermochromism or piezochromism. The green to yellow color change exhibited by the $[(C_2H_5)_2NH_2]_2CuCl_4$ crystal at $T_c = 50°C$ is associated with a SPT which modifies the $CuCl_4^{2-}$ structure from D_{4h} (square planar) to D_{2d} [9]. Recent hydrostatic pressure experiments carried out on $(CH_3CH_2NH_3)_2CdCl_4 : Cu^{2+}$ have shown the existence of piezochromism in this crystal [10]. The enormous redshift ($\Delta E = -1400\,cm^{-1}$) experienced by the first $Cl^- \rightarrow Cu^{2+}$ CT band at 26 kbar has been interpreted in terms of tetrahedral distortions of the nearly D_{4h} $CuCl_6^{4-}$ complex.

It is worth pointing out that CuX_6^{4-} usually displays an elongated D_{4h} symmetry with the exception of some fluoride crystals [4–7]. In chlorides, the only evidence of compressed $CuCl_6^{4-}$ was found in the layer perovskites $(enH_2)MnCl_4$ [11, 12] and $(C_nH_{2n+1}NH_3)_2MnCl_4$

($n = 1, 2$) [13] doped with Cu^{2+}. The deep red color of these crystals, associated with an intense absorption band at 21000 cm^{-1}, was interpreted in terms of a $Cl^-(eq) \rightarrow Cu^{2+}$ CT transition within a compressed D_{4h} symmetry molecular orbital (MO) framework. Such a geometry would be favoured by crystal anisotropy since this is the actual geometry of the replaced Mn^{2+} site. Recent work, however, performed on the $A_2Cd_{1-x}Mn_xCl_4 : Cu^{2+}$ (A = (CH_3NH_3) and $x = 0$–1) mixed crystals [13] has shown that: i) the CT spectra for the pure Mn and Cd crystals are completely different in spite of the fact that the same site symmetry is displayed by the Cd and Mn cations in these isomorphous crystals, ii) the oscillator strength of the CT bands increase by almost an order of magnitude on passing from $x = 0$ to $x = 1$. Furthermore, a new intense band around 21000 cm^{-1} appears for $x > 0$, its intensity being proportional to the Mn^{2+} concentration, x.

These findings suggest that the optical absorption (OA) spectra of these crystals could not be *only* related to structural modifications of the $CuCl_6^{4-}$ complex imposed by the host crystal but also some participation of the neighboring Mn^{2+} in the transition mechanism ought to be considered.

The aim of this work is to investigate the influence of Mn^{2+} in the OA spectra along the $A_2Cd_{1-x}Mn_xCl_4 : Cu^{2+}$ series. Special emphasis will be paid to the temperature dependence of the absorption bands as well as to the CF spectra whose bands strongly depend on the tetragonal distortion of $CuCl_6^{4-}$; i.e., the R_{ax}/R_{eq} parameter where R_{eq} and R_{ax} are the equatorial and axial Cl–Cu distances, respectively.

Throughout this work we demonstrate that the enhancement of intensity of the absorption bands associated with the Cu^{2+} impurities upon increasing the Mn concentration is due to the exchange interaction between Mn^{2+} and Cu^{2+} in Mn–Cu systems. Moreover, this exchange interaction is also responsible for the appearance of a new broad band at 21000 cm^{-1} and a narrow band at 25000 cm^{-1} in the $A_2Cd_{1-x}Mn_xCl_4 : Cu^{2+}$ crystals and therefore for the color change from light yellow to deep red on passing from $x = 0$ to $x = 1$. The temperature dependence of these bands is explained on the assumption of an effective spin-dependent transition mechanism acting on the exchange coupled Mn–Cu pairs. This mechanism originally proposed by Tanabe *et al.* [14] for explaining the intensity of the $^4A_1{}^4E$ Mn^{2+} excitations in Mn–Mn pairs, seems to describe properly this Mn^{2+} excitation in Mn–Cu systems [15–19].

A salient feature of the present work is the high oscillator strength found for the absorption bands. This is explained by the large transition moment associated with the first excited states of Mn^{2+} which are nearly resonant with CT states of the $CuCl_6^{4-}$ complex. The results of this work are compared with those available from other Mn–Cu exchange coupled systems in fluorides [15–17].

2. EXPERIMENTAL

Single crystals of $(CH_3NH_3)_2Cd_{1-x}Mn_xCl_4$ doped with $CuCl_2$ were grown by slow evaporation at 37°C from highly acidified (about 3M HCl) ethanol–water solutions containing stoichiometric amounts of $CH_3NH_2.ClH$ and the metallic chlorides with different $MnCl_2/CdCl_2$ concentration ratios. A nominal molar 1–10 mol % of the copper halide was added to the solutions. Suitable c-plates with edges parallel to the **a**, **b** and $\mathbf{a} \pm \mathbf{b}$ crystallographic directions were obtained.

The crystal structure was checked by powder X-ray diffraction. All crystals are orthorhombic (*Abma* space group) at room temperature. No trace of phase segregation has been observed for any Bragg peak in the mixed crystals. The intensity diagrams were analyzed by means of the FULLPROF software package [20]. The a, b and c parameters and the cell volume, V, obtained by fitting the experimental intensity to the calculated $I(2\theta)$ diagram, are given in Table 1. The fitting was largely improved taking into account preferential orientation in (0 0 1) planes. The Bragg R factors were smaller than 10%.

Precise measurements of the real Cu^{2+}, Mn^{2+} and Cd^{2+} concentrations were obtained by atomic absorption spectroscopy (Table 1). The real Mn^{2+} and Cu^{2+}

Table 1. Lattice parameters and cell volume of the $A_2Cd_{1-x}Mn_xCl_4 : Cu^{2+}$ series. The values of x as well as the real Cu^{2+} concentration have been obtained from atomic absorption. The number in parentheses indicates the standard deviation for a, b, c and V, and the nominal Cu^{2+} concentration added to solutions

x	a (Å)	b (Å)	c (Å)	V (Å^3)	mol % of Cu (nominal)
1.00	7.2701 (13)	7.2106 (12)	19.401 (2)	1016.9 (5)	0.50
0.97	7.2898 (13)	7.2255 (12)	19.385 (2)	1021.1 (5)	0.24 (1%)
0.85	7.3500 (18)	7.2690 (17)	19.329 (3)	1032.7 (7)	0.20 (1%)
0.42	7.4129 (16)	7.3291 (16)	19.279 (3)	1047.4 (6)	1.09 (10%)
0.31	7.4226 (14)	7.3350 (14)	19.278 (2)	1049.6 (5)	0.14 (1%)
0.04	7.481 (2)	7.382 (2)	19.249 (4)	1063.0 (8)	1.62 (10%)
0.00	7.485 (2)	7.390 (2)	19.245 (4)	1064.5 (8)	–

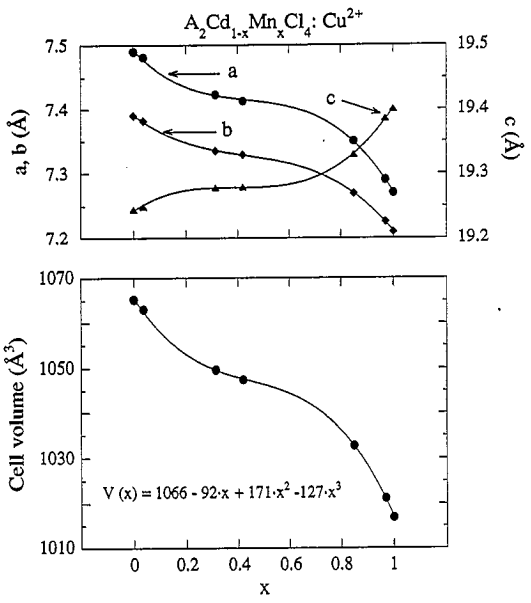

Fig. 1. Variation of the orthorhombic **a**, **b** and **c** cell parameters (top) and the cell volume (bottom) with the Mn concentration, x, along the $A_2Cd_{1-x}Mn_xCl_4$ series. The full lines represent the least-square fitting of data to a polynomial of order 3.

concentration in the crystals are about a factor 5 and 10 less than the nominal concentrations in solutions, respectively.

The variation of the lattice parameters and the cell volume with x for the $A_2Cd_{1-x}Mn_xCl_4$ series is shown in Fig. 1. Note that $V(x)$ significantly deviates from Vegard's law. The variation of the cell volume can be described by a polynomial of order 3 in the 0–1 range as $V(x) = 1066 - 92x + 171x^2 - 127x^3$. A similar behavior is also found for the a, b and c parameters.

The crystals were oriented and selected for optical studies by means of a polarizing microscope. The refractive index in the crystal layer was measured by the Becke line method using calibrated Cargille liquids.

Spectra were recorded with a Lambda 9 Perkin Elmer spectrophotometer equipped with Glan Taylor polarizing prisms. Sample path lengths for absorption were about 0.1–1 mm. The temperature was stabilized to within 0.05 K in the 9.5–300 K range with a Scientific Instruments 202 closed-circuit cryostat and an APD-K controller. For higher temperatures (300–550 K), a Leica heating stage was employed.

3. RESULTS

Figure 2 depicts the polarized OA spectra at 9.5 K of the $A_2Cd_{1-x}Mn_xCl_4 : Cu^{2+}$ series for $x = 0$, 0.3 and 1. The evolution of the spectra clearly shows both the enhancement of band intensity and the spectral changes upon increasing the Mn^{2+} concentration. The polarized OA spectra along the three orthorhombic **a**, **b** and **c** directions for $A_2CdCl_4 : Cu^{2+}$ at

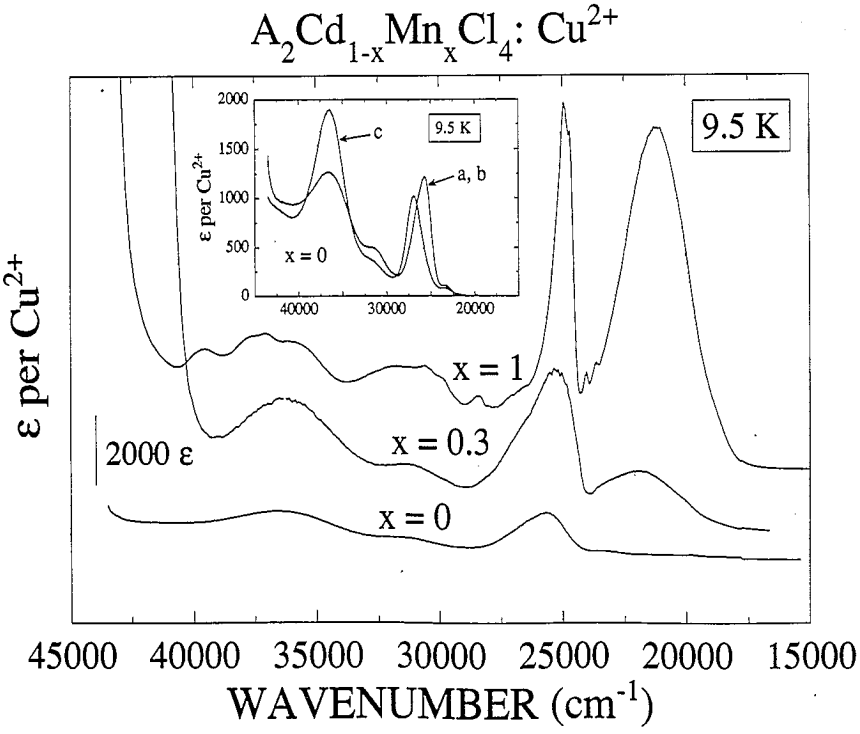

Fig. 2. Polarized optical absorption spectra at $T = 9.5$ K corresponding to the $x = 0$, 0.3 and 1 crystals of the $A_2Cd_{1-x}Mn_xCl_4 : Cu^{2+}$ series. The spectra are polarized along the **a** and **b** directions. The inset shows the corresponding spectra for $x = 0$ along the three orthorhombic directions.

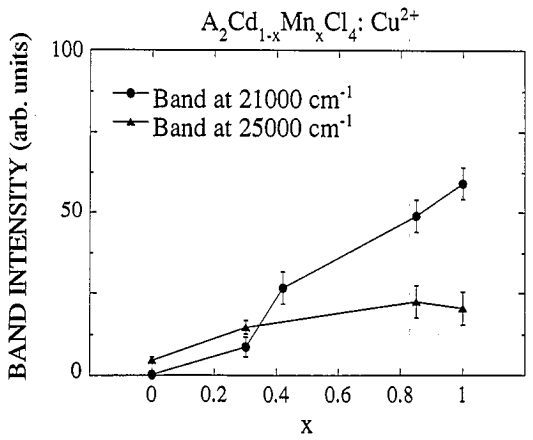

Fig. 3. Plot of the room temperature integrated band intensity versus x for the 21000 and 25000 cm^{-1} bands. The intensity has been obtained from optical spectra scaled to molar extinction values per Cu.

$T = 9.5$ K are given in the inset. The tail of the first band at 25000 cm^{-1} for $x = 0$ is responsible for the yellow color of the Cd crystals whereas the strong band at 21000 cm^{-1} observed for $x = 1$ is responsible for the deep red color exhibited by the Mn crystal. Intermediate colors are observed between $x = 0$ and $x = 1$. The occurrence of a new band below 25000 cm^{-1} is related to the presence of Mn^{2+} in the host crystal. As Fig. 3 shows, the intensity of this new band at 21000 cm^{-1} as well as the band at 25000 cm^{-1} is proportional to the real Mn^{2+} concentration, x. The corresponding room temperature CF spectra in the NIR region for $x = 0$ and $x = 1$ and the spectrum of the pure $(CH_3NH_3)CuCl_4$ crystal are shown in Fig. 4. It must be observed that the highest energy band located around 13000 cm^{-1} in the pure Cu crystal appears at lower energies in the Cd and Mn crystals (11000 cm^{-1}). The fact that we observe a similar CF spectrum for Cd and Mn in spite of the big differences exhibited by the corresponding CT spectra is worth noting. This feature is of great interest since similar spectral differences found in the CF spectra of $(enH_2)MnCl_4 : Cu^{2+}$ and $(enH_2)CuCl_4$ were a key argument to discard the presence of D_{4h} elongated $CuCl_6^{4-}$ complexes in the Mn crystal [12].

Figure 5 illustrates the variation of OA spectra for the $A_2MnCl_4 : Cu^{2+}$ crystal with temperature. It is important to observe that this thermal behavior is quite different from that found for the $A_2CdCl_4 : Cu^{2+}$ whose band intensity does not experience significant variations with temperature. Figures 6 and 7 show the variation of the oscillator strength and transition energy corresponding to the first absorption bands with the temperature. The oscillator strength has been obtained from the integrated intensity of the absorption band through the equation [21]:

$$f = 3.89 \times 10^{-8} \frac{n}{(n^2+2)^2} \int \epsilon dE \qquad (1)$$

where ϵ is the molar extinction coefficient and E is the

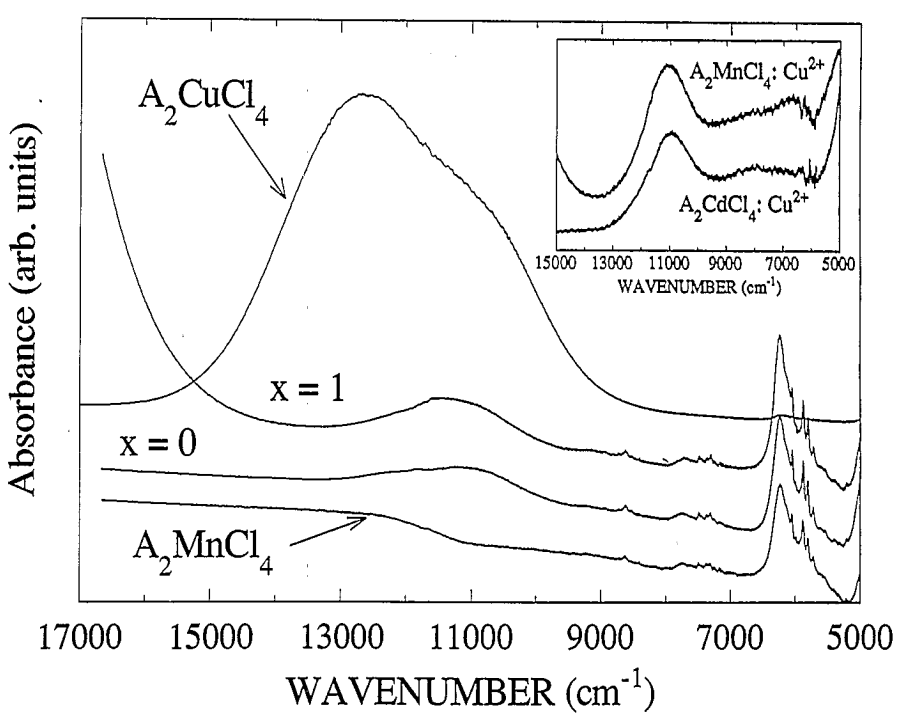

Fig. 4. Polarized optical absorption spectra in the NIR region at room temperature of the A_2CuCl_4, $A_2Cd_{1-x}Mn_xCl_4 : Cu^{2+}$ for $x = 0$ and $x = 1$, and the Cu^{2+} undoped A_2MnCl_4. The latter spectrum is given for comparison purposes. The inset shows the spectra corresponding to the $A_2MnCl_4 : Cu^{2+}$ and $A_2CdCl_4 : Cu^{2+}$ to which the spectrum of the pure A_2MnCl_4 has been subtracted in order to obtain the contribution from Cu^{2+}.

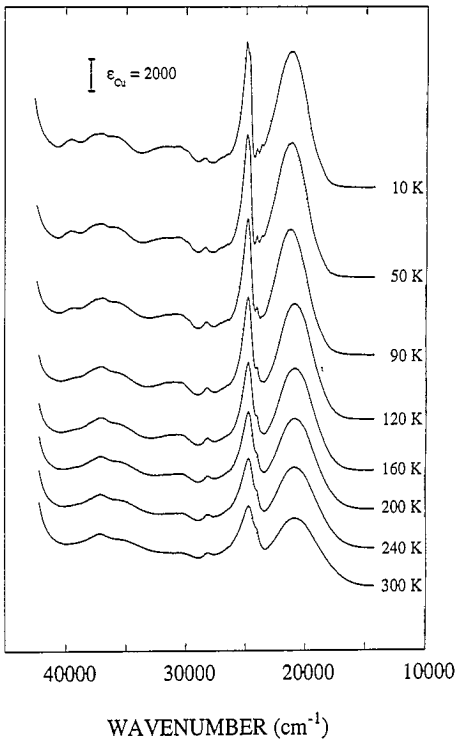

Fig. 5. Temperature dependence of the OA spectra for $A_2MnCl_4 : Cu^{2+}$. Note the spectral variations around the structural phase transition temperature, $T_{cl} = 92$ K, of the host crystal.

transition energy (cm^{-1}). The refractive index within the layer is $n = 1.61$ for both the $x = 1$ and $x = 0$ crystals.

Figure 8 shows the variation of the crystal absorbance at 700 mn in the 9.5–300 K range for the three selected crystals. Such a variation is a good probe for detecting SPT in the host crystals through the abrupt changes exhibited by the crystal transmittance at critical temperatures. Apart from the abrupt changes undergone by these parameters around the SPT temperatures, it must be observed the different temperature dependence undergone by the oscillator strength, $f(T)$, along the series (Fig. 6). Whereas $f(T)$ does not exhibit significant variations in the whole 9.5–300 K range for the Cd crystal, it continuously decreases upon increasing temperature in the mixed and pure Mn crystals. However, an anomalous behavior of $f(T)$ is observed between 80 and 150 K for $x = 0.3$.

The variation of the transition energy $E(T)$ shows an important redshift above the SPT temperature T_{cl}, for $x = 0.3$ and $x = 1$ [22–25]. The temperature dependence of the bandwidth, $H(T)$, corresponding to the 21000 cm^{-1} band for $x = 1$ (Fig. 5) can be described by means of usual functions of the type [26]: $H(T) = H_0[\coth(\hbar\omega_{eff}/2kT)]^{1/2}$ with an effective vibrational energy $\hbar\omega_{eff} = 208$ cm^{-1} and a $T = 0$ K, bandwidth, $H_0 = 3100$ cm^{-1}.

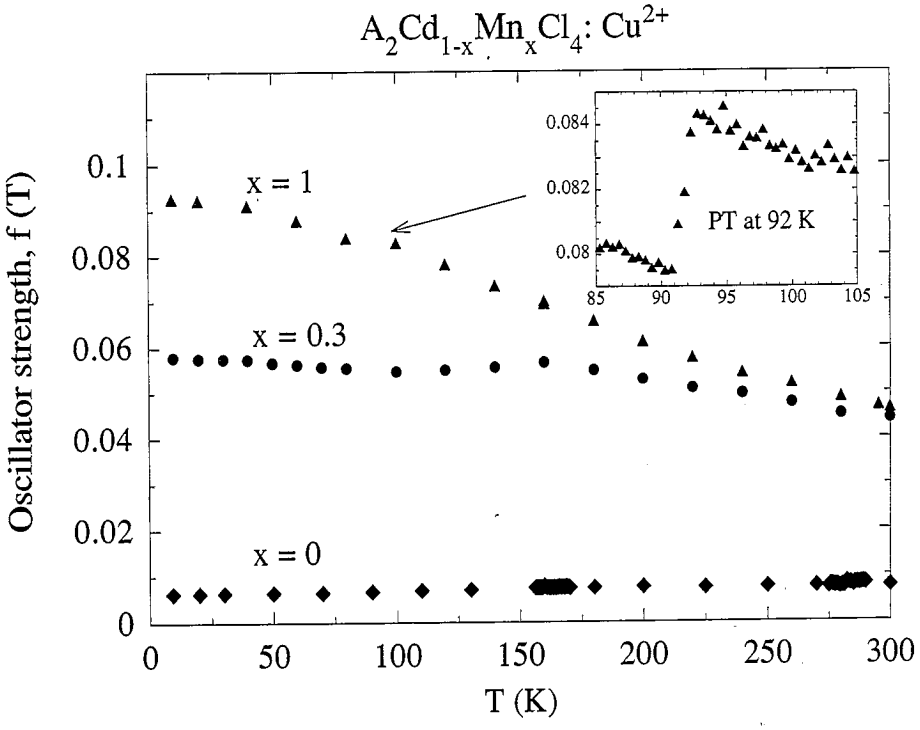

Fig. 6. Variation of the oscillator strength with temperature, $f(T)$, for the three selected crystals $x = 0$, 0.3 and 1 of the series. The oscillator strength has been obtained from the integrated band intensity through eqn (1). $f(T)$ corresponds to the 21000 cm^{-1} band for $x = 1$, the sum of the 21000 and 25000 cm^{-1} bands for $x = 0.3$, and the 25000 cm^{-1} for $x = 0$. We give the total oscillator strength of the two bands for $x = 0.3$ due to difficulties to separate both contributions above 100 K. The inset shows a magnification of $f(T)$ around the SPT at $T_{cl} = 92$ K.

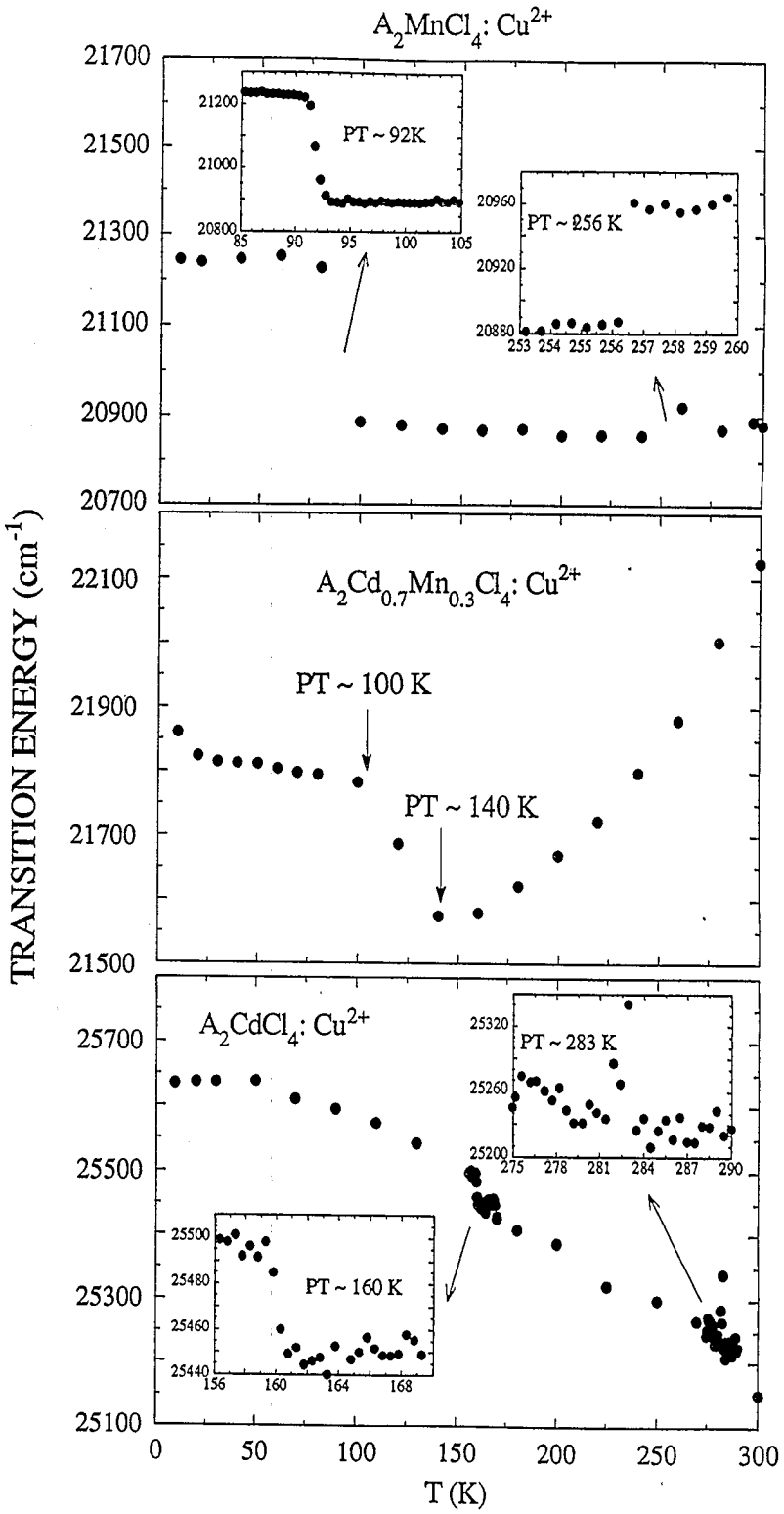

Fig. 7. Temperature dependence of the transition energy corresponding to the first Charge Transfer band in different crystal of the $A_2Cd_{1-x}Mn_xCl_4 : Cu^{2+}$ series. The transition energies have been derived from moment analysis. The insets show those variations around the structural phase transition temperatures. The first order character of these transitions are reflected by the abrupt jumps experienced by $E(T)$ at the critical temperatures.

Table 2. Transition energy (cm^{-1}), Polarization and Oscillator Strength, f, corresponding to the charge transfer bands of several $A_2Cd_{1-x}Mn_xCl_4 : Cu^{2+}$ crystals ($x = 1, 0.3$ and 0). The assignment is made within a D_{2h} scheme of the $CuCl_6^{4-}$ complex. Elongated and compressed D_{4h} symmetry are also considered. **a**, **b** and **c** denote the orthorhombic directions; x, y and z are the local coordinate axes of the complex with z taken along the fourfold axis. The polarization is given in parentheses

Transition assignment			$A_2CdCl_4 : Cu^{2+}$		$A_2Cd_{0.7}Mn_{0.3}Cl_4 : Cu^{2+}$		$A_2MnCl_4 : Cu^{2+}$	
D_{4h} elongated $^2B_{1g}\ (x^2-y^2)\rightarrow$	D_{2h} intermediate $^2A_g[\alpha(x^2-y^2)+\beta z^2]\rightarrow$	D_{4h} compressed $^2A_{1g}\ (z^2)\rightarrow$	Observed energy $T = 9.5$ K	f	Observed energy $T = 9.5$ K	f	Observed energy $T = 9.5$ K	f
$^2A_{2u}$ (ax; $\pi+\sigma$) (F)	$^2B_{1u}$ (z)	^2E_u (x, y)	23150 (a, b, c)	10^{-4}	21900 (a, b)	2.10^{-2}	21250 (a, b)	9.10^{-2}
^2E_u (eq; $\pi+\sigma$) (x, y)	$^2B_{2u}$ (y)	$^2A_{2u}$ (z)	25700 (a, b)	8.10^{-3}	25250 (a, b)	3.10^{-2}	24900 (a, b)	3.10^{-2}
	$^2B_{3u}$ (x)		26950 (c)	7.10^{-3}			26900 (c)	$\sim 5.10^{-2}$†
$^2B_{2u}$ (π) (z)	$^2B_{1u}$ (z)	^2E_u (x, y)						
^2E_u (ax; π) (x, y)	$^2B_{2u}$ (y)	$^2B_{2u}$ (F)	31400 (a, b)	5.10^{-4}			31900 (a, b)	$\sim 10^{-2}$
	$^2B_{3u}$ (x)							
^2E_u (eq; $\sigma+\pi$) (x, y)	$^2B_{2u}$ (y)	$^2A_{2u}$ (z)	36500 (a, b)	10^{-2}	36400 (a, b)		36100 (a, b)	$\sim 10^{-2}$
	$^2B_{3u}$ (x)		36500 (c)	2.10^{-2}				
$^2A_{2u}$ (eq; $\sigma+\pi$) (F)	$^2B_{1u}$ (z)	^2E_u (x, y)					36100 (c)	$\sim 10^{-2}$†

†Data from Ref. [12].
F denotes forbidden transition.

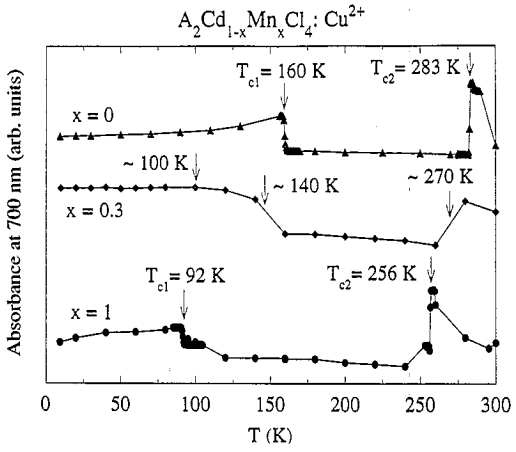

Fig. 8. Variation of the absorbance at 700 nm with temperature for $x = 0$, 0.3 and 1 in $A_2Cd_{1-x}Mn_xCl_4:Cu^{2+}$. Note that the anomalies observed at the phase transition temperatures are completely due to changes of the crystal bulk transmittance since no absorption from Cu^{2+} occurs at this wavelength.

Tables 1 and 2 collect some relevant structural and spectroscopic data of the $A_2Cd_{1-x}Mn_xCl_4:Cu^{2+}$ series. The band assignment given in Table 2 will be analyzed in the following section.

4. ANALYSIS AND DISCUSSION

4.1. *Local structure of the* $CuCl_6^{4-}$ *complex along the* $A_2Cd_{1-x}Mn_xCl_4:Cu^{2+}$ *series*

4.1.1. *Analysis of the charge transfer of* $CuCl_6^{4-}$ *in* $A_2CdCl_4:Cu^{2+}$. The $CuCl_6^{4-}$ molecular unit is the basis for explaining the OA spectra of the $A_2Cd_{1-x}Mn_xCl_4:Cu^{2+}$ series, since this is the coordination of the substituted Cd or Mn cations. Furthermore, the $CuCl_6^{4-}$ symmetry should be nearly D_{4h} compressed if the actual Cd or Mn site symmetry is kept after Cu replacement [27, 28]. In fact, the site symmetry was an important argument to claim for a compressed D_{4h} symmetry for $CuCl_6^{4-}$ in $(enH_2)MnCl_4:Cu^{2+}$, in order to explain the position and polarization of the first CT band at 20800 cm^{-1} [12]. Nevertheless, this symmetry should be even more favored in the isomorphous A_2CdCl_4 crystal where the $CdCl_6^{4-}$ tetragonal compression is more pronounced than that for the $MnCl_6^{4-}$ in A_2MnCl_4. The in-plane equatorial distance, R_{eq}, and the out of plane axial distance, R_{ax}, in the perfect crystal are $R_{eq} = 2.64$ and 2.56 Å, and $R_{ax} = 2.54$ and 2.50 Å for A_2CdCl_4 [27] and A_2MnCl_4 [28], respectively. However, this does not seem to be the situation encountered for $CuCl_6^{4-}$ in the Cd crystal after the analysis of the CT spectra performed in [13] and confirmed by the CF spectra reported in this work. Moreover, the position and polarization of the CT bands likely indicates that the $CuCl_6^{4-}$ complex displays a nearly D_{4h} elongated symmetry, with the long axial bond randomly directed either along the [1, 1, 0] or [1, −1, 0] directions within the (0 0 1) basal plane. This arrangement resembles the antiferrodistortive structure displayed by the D_{4h} elongated $CuCl_6^{4-}$ complexes in the pure A_2CuCl_4 crystal, where the axial bond in one Cu corresponds to the equatorial bond of the nearest Cu [29, 30]. The present conclusion is based on the fact that the CT spectra of $A_2CdCl_4:Cu^{2+}$ (inset of Fig. 2) show two bands at 25700 cm^{-1} in **a**, **b** polarization (26950 cm^{-1} in **c** polarization) and at 36500 cm^{-1}, which are characteristic of CT transitions from the bonding e_u $(\pi+\sigma)$ and e_u $(\sigma+\pi)$ mainly equatorial Cl^- levels to the mainly antibonding Cu^{2+} b_{1g} (x^2-y^2) molecular orbital within an elongated D_{4h} symmetry molecular framework for $CuCl_6^{4-}$ [13]. The polarization of these bands together with the similitude of the CT spectra of $A_2CdCl_4:Cu^{2+}$ and $CdCl_2:Cu^{2+}$, where $CuCl_6^{4-}$ displays an elongated D_{4h} symmetry [31], allow us to conclude that the actual complex symmetry is nearly D_{4h} elongated instead of D_{4h} compressed. The fact that these two CT bands are observed in the three polarizations and the intensity of the 36500 cm^{-1} band along **c** is twice as the intensity along **a** or **b**, clearly indicates that the equatorial plane of the complex must involve two Cu–Cl bonds in the **c**-plane and two terminal Cu–Cl bonds along **c**. The isotropy displayed by the CT and CF spectra in the **c**-plane (**a** and **b** polarizations) suggests that the axial Cu–Cl bonds of a given complex are either parallel or perpendicular to the axial bonds of other $CuCl_6^{4-}$ units.

4.1.2. *Correlation between the local structure and the crystal field spectra in* $CuCl_6^{4-}$. The comparison between the CF spectra of $A_2MnCl_4:Cu^{2+}$, $A_2CdCl_4:Cu^{2+}$ shown in Fig. 4 and the corresponding spectrum of $CdCl_2:Cu^{2+}$ also confirms the elongated D_{4h} symmetry for $CuCl_6^{4-}$ in the three crystals. The three bands observed in $CdCl_2:Cu^{2+}$ at 11000, 9500 and 6400 cm^{-1} are assigned to CF transitions from the mainly Cu^{2+} $e_g(xz, yz)$, $b_{2g}(xy)$ and $a_{1g}(3z^2-r^2)$ one electron levels to the unfilled highest energy $b_{1g}(x^2-y^2)$ one [32]. In our case, we observe the highest energy band at 11300 cm^{-1} while the band around 9500 cm^{-1}, as in $CdCl_2:Cu^{2+}$, is hidden in the room temperature spectra. The lowest energy band probably overlaps with the vibrational overtones of the $(CH_3NH_3)^+$ organic groups. The inset of Fig. 4 shows the OA spectrum of these crystals in which the contribution from the organic groups has been subtracted employing the OA spectrum of the undoped crystals. A broad band is observed around 8000 cm^{-1} and 7000 cm^{-1} for $A_2CdCl_4:Cu^{2+}$ and $A_2MnCl_4:Cu^{2+}$, respectively. Although these bands are probably associated with the first $a_{1g}(3z^2-r^2) \rightarrow b_{1g}(x^2-y^2)$ (D_{4h} scheme) CF band, a

Table 3. Some relevant structural and spectroscopic data for several Cu(II) chlorides. R_{eq} and R_{ax} are the equatorial and axial Cu–Cl distances of the $CuCl_6^{4-}$ complexes. The first three compounds correspond to square planar $CuCl_4^{2-}$ complexes. The ϵ_1, ϵ_2 and ϵ_3 parameter are the transition energies obtained from the crystal field spectra (Fig. 10). The energy of the totally symmetric stretching vibrations are given for two $CuCl_4^{2-}$ complexes and for one $CuCl_6^{4-}$ complex. The two energies for $(cyclamH_4)CuCl_6$ correspond to the stretching vibration of the equatorial and axial ligands, respectively. The experimental data were taken from references given in the last row

Compound	R_{eq} (Å)	R_{ax} (Å)	$\epsilon_1 = \Delta_e$ (cm^{-1})	$\epsilon_2 = 10Dq$ (cm^{-1})	ϵ_3 (cm^{-1})	$\hbar\omega$ (cm^{-1})	Ref.
$C_{42}H_{56}N_2O_2CuCl_4$	2.26	–	16600	12200	14000	–	46, 47, 48
$(nmpH_2)CuCl_4$	2.27	–	16900	12500	14500	276	49, 50, 51
$(creatinium)_2CuCl_4$	2.25	–	16500	12300	14000	290	52, 48
$CsCuCl_3$	2.32	2.78	8300	10000	12930	–	53, 54
$(EtNH_3)_2CuCl_4$	2.29	3.04	11130	12390	13290	–	55, 56
$(n\text{-}PrNH_3)_2CuCl_4$	2.28	3.04	11300	12300	13500	–	56, 57
$(MetNH_3)_2CuCl_4$	2.28	2.98	11090	12110	13210	–	29
$(cyclamH_4)CuCl_6$	2.29	3.17	13400	11100	12400	262/101	23
$[Pt(NH_3)_4]CuCl_4$	2.29	3.26	14300	10900	13100	–	58, 59
$CdCl_2 : Cu^{2+}$	–	–	6400	9500	11000	–	32
$A_2CdCl_4 : Cu^{2+}$	–	–	(8000?)	9000 shoulder	11300	–	Present work
$A_2MnCl_4 : Cu^{2+}$	–	–	(7000?)	9000 shoulder	11300	–	Present work
$(enH_2)MnCl_4 : Cu^{2+}$	–	–	–	9000	11300	–	12

precise measurement of this transition energy is not possible due to procedure employed for obtaining such OA spectra. Since the CF spectra of $A_2MnCl_4 : Cu^{2+}$ and $A_2CdCl_4 : Cu^{2+}$ are very similar to that of $CdCl_2 : Cu^{2+}$, this strongly suggests that the Cu^{2+} local structure is also similar for the three crystals, in spite of the huge differences exhibited by the CT spectrum in **a** and **b** polarizations for the Mn crystal (Fig. 2). However, the CT spectra for the Mn and Cd crystals along **c** also support an elongated D_{4h} symmetry for $CuCl_6^{4-}$ in the Mn crystal since the same **c** polarized bands associated with electronic transitions mainly involving terminal Cu–Cl bonds are observed [12, 13].

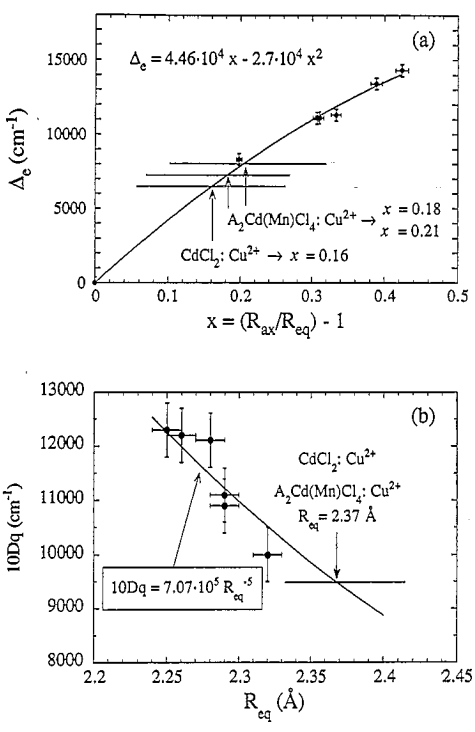

Fig. 9. Spectroscopic and structural correlation in $CuCl_6^{4-}$ complexes: Plot (a) shows the variation of the tetragonal splitting, $\Delta_e = E[^2A_{1g}\ (3z^2-r^2)] - E[^2B_{1g}\ (x^2-y^2)]$, with the tetragonal distortion parameter, $x = (R_{ax}/R_{eq}) - 1$ for several $CuCl_6^{4-}$ complexes of D_{4h} symmetry. Plot (b) shows the variation of $10Dq = E[^2B_{2g}(xy)] - E[^2B_{1g}\ (x^2-y^2)]$, with the equatorial Cu–Cl distance, R_{eq}. Experimental data were taken from Table 3. Full lines are the least-square fittings to a quadratic function for $\Delta_e(x)$ in (a), and a power law as $10Dq = K R_{eq}^{-5}$ in (b). The vertical arrows and horizontal lines indicate the values of Δ_e and 10Dq and the corresponding x and R_{eq} parameters, respectively, for $CdCl_2 : Cu^{2+}$, $A_2MnCl_4 : Cu^{2+}$ and $A_2CdCl_4 : Cu^{2+}$.

At this stage, there must be an explanation for the different experimental CF energies observed for the pure A_2CuCl_4 crystal and the Cu^{2+} doped A_2MnCl_4, A_2CdCl_4 and $CdCl_2$ crystals. As suggested by McDonald and Hitchman [33], the difference between these spectra probably reflects slight variations of the tetragonal distortion of the $CuCl_6^{4-}$ units. Table 3 collects the experimental transition energies obtained from the CF spectra of some pure Cu compounds where the axial and equatorial bond lengths are known from X-ray diffraction. Figure 9 plots the variation of the splitting of the parent e_g octahedral levels, Δ_e, and the parameter 10Dq as a function of the tetragonal distortion defined as $x = (R_{ax}/R_{eq}) - 1$ and R_{eq}, respectively, for the crystal series given in Table 3. The correlation between structural data and spectroscopic parameters allows us to confirm the proposed D_{4h} elongated symmetry for the present $CuCl_6^{4-}$ and also justifies the occurrence of such a symmetry in the layer perovskites with compressed sites.

Within an angular overlap model (AOM) [1], the spectroscopic parameters: $\Delta_e = \epsilon_1$, $\Delta_t = \epsilon_3 - \epsilon_2$ and $10Dq(eq) = \epsilon_2$, where ϵ_1, ϵ_2 and ϵ_3 are the CF transition energies (Fig. 10), are given in terms of the e_σ and e_π bonding parameters by $\Delta_e = 2e_\sigma(eq) - 2e_\sigma(ax)$ and $\Delta_t = 2e_\pi(eq) - 2e_\pi(ax)$. The parameter 10Dq(eq) only

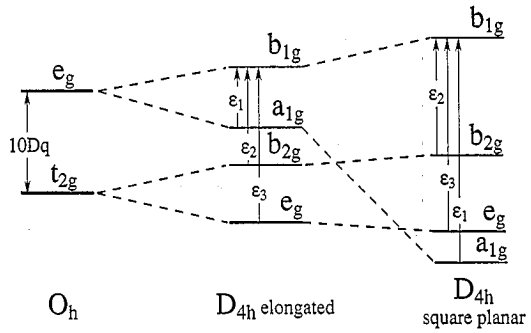

Fig. 10. Correlation diagram corresponding to a $CuCl_6^{4-}$ complex from octahedral (O_h) to square planar (D_{4h}) symmetry, passing through an elongated (D_{4h}) intermediate. ϵ_1, ϵ_2 and ϵ_3 represent the three crystal field transition observed in the OA spectra.

depends on the equatorial distance R_{eq}. For a fixed value of R_{eq}, parameters Δ_e and Δ_t change from $2e_\sigma(eq)$ and $2e_\pi(eq)$, respectively, for a square planar $CuCl_4^{2-}$ complex ($R_{ax} \to \infty$) to zero when $R_{ax} = R_{eq}$. The value of Δ_e is higher than Δ_t due to the higher interactions from the σ bonding electrons than those from the π-ones. Ratios of Δ_e/Δ_t of about 3–4 have been experimentally observed for MnF_6^{3-} and CuF_6^{4-} complexes [34]. For $CuCl_6^{4-}$, the CF spectra are similar to those found for square planar $CuCl_4^{2-}$ whenever the axial Cu–Cl distance is longer than 3.20 Å [33]. Below this distance, Δ_e decreases upon decreasing R_{ax}. This effect is well illustrated in the plot of Fig. 9. Estimates on the local structure of $CuCl_6^{4-}$ for doped crystals can be extracted from Fig. 9 through the CF transition energies. Using the Δ_e values of Table 3, we obtain ratios of $R_{ax}/R_{eq} = 1.16$, 1.18 and 1.21 for $CdCl_2:Cu^{2+}$, $A_2MnCl_4:Cu^{2+}$ and $A_2CdCl_4:Cu^{2+}$, respectively. These values together with R_{eq} derived from 10Dq on the assumption that $10Dq \propto R_{eq}^{-5}$ allow us to obtain $R_{eq} = 2.37$ Å for the three systems while $R_{ax} = 2.75$, 2.80 and 2.87 Å for $CdCl_2:Cu^{2+}$, $A_2MnCl_4:Cu^{2+}$ and $A_2CdCl_4:Cu^{2+}$, respectively. These distances are in agreement with those obtained for $CdCl_2:Cu^{2+}$ through MS–Xα calculations and the analysis of the isotropic superhyperfine tensor ($R_{ax} = 2.80$ Å; $R_{eq} = 2.35$ Å) [35], and thus confirm the elongated symmetry for $CuCl_6^{4-}$ in $A_2CdCl_4:Cu^{2+}$ and $A_2MnCl_4:Cu^{2+}$.

This result indicates that the strength of the Cu–Cl bond is more important than the corresponding Cd–Cl or Mn–Cl bond strength for the equilibrium geometry even though the host site tends to impose a compressed geometry for $CuCl_6^{4-}$.

4.1.3. *Local structure of* $CuCl_6^{4-}$ *from vibrational* Cu–Cl *frequencies.* The local structure for $CuCl_6^{4-}$ in $A_2CdCl_4:Cu^{2+}$ and $A_2MnCl_4:Cu^{2+}$ derived in the previous section could also be anticipated from the analysis of the vibrational frequencies of the totally symmetric modes associated with the Cd–Cl, Mn–Cl and Cu–Cl bonds. If the M–Cl bonds are considered within the (0 0 1) plane of the perovskite layer as a system of coupled springs whose force constants are derived from the vibrational angular frequency by $k = m\omega^2$, then the equilibrium Cu–Cl distances for the $CuCl_6^{4-}$ impurity can be obtained by requiring that the internal force acting on the shared Cl^- ion is zero:

$$k_1^{eq}(R_i^{eq} - R_{Cu-Cl}^{eq}) = k_i\left(\frac{R_{0i}}{2} - R_i^{eq}\right)$$
$$k_1^{ax}(R_{Cu-Cl}^{ax} - R_i^{ax}) = k_i\left(R_i^{ax} - \frac{R_{0i}}{2}\right) \qquad (2)$$

for the equatorial and axial Cu–Cl bonds, respectively. k_1^{eq} and k_1^{ax} are the corresponding force constants, and k_i with $i = 1$ and 2 is the Cd–Cl and Mn–Cl force constant, respectively. R_{Cu-Cl}^{eq} and R_{Cu-Cl}^{ax}, are the equilibrium distances in a pure Cu compound, and R_i^{eq} and R_i^{ax} are the corresponding ones in A_2CdCl_4 ($i = 1$) and A_2MnCl_4 ($i = 2$). R_{0i} is the nearest M–Cu (M = Cd, Mn) distance within the (0 0 1) plane. Then R_i^{eq} and R_i^{ax} can be estimated from the structural data and the proper vibrational frequencies available for several $CuCl_4^{2-}$ and $CuCl_6^{4-}$ complexes (Table 3), and for the Mn–Cl and Cd–Cl bonds. Taking values $\hbar\omega = 290$ and 101 cm^{-1} for the stretching vibration associated with the equatorial ($R_{eq} = 2.25$ Å) and axial ($R_{ax} = 3.2$ Å) Cu–Cl bonds, respectively, $\hbar\omega = 210\,cm^{-1}$ for Mn–Cl in Na_6MnCl_8 [36, 37] and $CdCl_2:Mn^{2+}$ [38] and $\hbar\omega = 220\,cm^{-1}$ for Cd–Cl in Na_6CdCl_8 [36] and A_2CdCl_4 [39], we obtain from eqn (2): $R_{ax} = 2.7$ Å and $R_{eq} = 2.4$ Å for $A_2MnCl_4:Cu^{2+}$ and $A_2CdCl_4:Cu^{2+}$. Assuming that the equilibrium distance of the terminal Cu–Cl bond is $R_{eq} = 2.3$ Å, the real local structure around the Cu is orthorhombic D_{2h} (nearly D_{4h}) like it must correspond to a complex formed in an orthorhombic host. Note that these estimates are similar to those obtained from the CF spectrum analysis and therefore the present geometrical description for $CuCl_6^{4-}$ is likely. This analysis suggests that a compressed D_{4h} symmetry might be obtained in this kind of layered structures whenever the bonding strength of the host cations is stronger than the corresponding Cu bonding. The compressed geometries found in several fluorides seems to follow this trend [3–8].

4.2. *Influence of Mn in the optical absorption spectra of* $A_2Cd_{1-x}Mn_xCl_4:Cu^{2+}$

4.2.1. *Enhancement of band intensity in exchange coupled* Mn–Cu *systems.* We associate the enhancement of intensity and the presence of new bands in the OA spectra along the $A_2Cd_{1-x}Mn_xCl_4:Cu^{2+}$ series with exchange coupled Mn–Cu systems rather than with isolated $CuCl_6^{4-}$ complexes. Two fundamental

features exclude the latter possibility: i) the geometrical structure of the $CuCl_6^{4-}$ complex formed in $A_2MnCl_4 : Cu^{2+}$ and $A_2CdCl_4 : Cu^{2+}$ are nearly the same according to the previous discussion. In such a case, the CT spectra of the Mn crystal should be similar to that of $CdCl_2 : Cu^{2+}$ and $A_2CdCl_4 : Cu^{2+}$, ii) even though the $CuCl_6^{4-}$ symmetry was nearly D_{4h} compressed ($R_{eq} = 2.5$–2.6 Å and $R_{ax} \sim 2.3$ Å), the presence of an in-plane polarized narrow band at 25000 cm^{-1} could not be accounted for within this scheme. According to the analysis performed by Schmid *et al.* [12], such a band resembles the $^6A_1 \rightarrow {}^4E$, $^4A_1$ spin–flip Mn^{2+} excitation in $MnCl_6^{4-}$. However its oscillator strength is enormously high ($f = 3 \times 10^{-2}$) to be assigned to a single Mn^{2+} pair excitation. Furthermore, the oscillator strength of the broad band at 21000 cm^{-1} ($f = 9 \times 10^{-2}$) which was assigned to the $e_u(\pi + \sigma) \rightarrow a_{1g}(3z^2 - r^2)$ CT transition in a compressed D_{4h} symmetry [11, 12], is about one order of magnitude higher than the corresponding first CT band in $A_2CdCl_4 : Cu^{2+}$ ($f = 8 \times 10^{-3}$). This difference is hard to conciliate with the longer equatorial distance displayed by the compressed centers. In fact, the overlap between the $e_u(\pi + \sigma)$ and $a_{1g}(3z^2 - r^2)$ wavefunctions must be much smaller than the overlap between the $e_u(\pi + \sigma)$ and $b_{1g}(x^2 - y^2)$ levels for elongated complexes, and therefore weaker oscillator strengths should be expected for these CT transitions in compressed centers. Moreover, the intensity of the 21000 cm^{-1} band for $A_2MnCl_4 : Cu^{2+}$ continuously decreases by about 40% from 9.5 to 500 K (Figs 5, 6 and 11) whereas no significant change of intensity is observed for the first CT band in $A_2CdCl_4 : Cu^{2+}$. Consequently, the narrow and broad bands at 25000 and 21000 cm^{-1} observed in $A_2MnCl_4 : Cu^{2+}$ must be associated with exchange coupled Mn–Cu systems. Although exchange coupled systems involving Mn–Cu dimers or Cu–Mn–Cu trimers have been investigated in fluoride crystals such as $KZnF_3 : Mn^{2+}$, Cu^{2+} [15, 16], $K_2CuF_4 : Mn^{2+}$ [17] and in organometallic systems [18, 19], the effects of these interactions are usually studied through the fine spectral features observed around the *single* $^6A_1 \rightarrow {}^4E\,{}^4A_1$ spin–flip transition of Mn^{2+} as well as through their thermal dependence. Valuable information on the exchange constants for both the ground and the excited states can be extracted from the optical spectra. It is worth noting the high values of the ground state exchange constant measured spectroscopically in the Mn–F–Cu systems formed in $K_2CuF_4 : Mn^{2+}$ ($J = 25\,cm^{-1}$) [17] and $KZnF_3 : Mn^{2+}$, Cu^{2+} ($J = 65\,cm^{-1}$) [15]. The exchange constants are given on the basis of an exchange hamiltonian defined as $H_{ex} = 2J\mathbf{S}_{Mn}.\mathbf{S}_{Cu}$. These J values are about one order of magnitude

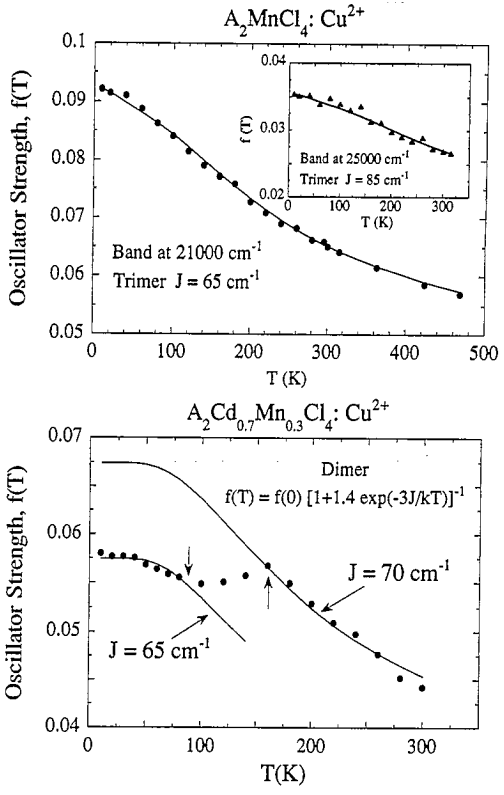

Fig. 11. Temperature dependence of the oscillator strength corresponding to bands at 25000 and 21000 cm^{-1} (inset) measured in $A_2MnCl_4 : Cu^{2+}$ and the two bands measured in $A_2Cd_{0.7}Mn_{0.3}Cl_4 : Cu^{2+}$. Full lines represent the least-square fitting of the experimental $f(T)$ data to eqn (5) for $A_2MnCl_4 : Cu^{2+}$ and to eqn (4) for $A_2Cd_{0.7}Mn_{0.3}Cl_4 : Cu^{2+}$. In this latter case we fit the experimental curve below 80 K and above 150 K (see text for explanation). The small jump observed in Fig. 6 at $T_{c1} = 92$ K has been corrected for this analysis.

higher than the antiferromagnetic exchange interaction of the $RbMnF_3$ bulk ($J = 3.4\,cm^{-1}$) [40] or the ferromagnetic one in K_2CuF_4 ($J = -8.8\,cm^{-1}$) [41] obtained from inelastic neutron scattering and specific heat measurements, respectively. Furthermore, the exchange interaction between the $^4A_1$ excited state of Mn^{2+} and the ground state of Cu^{2+} is ferromagnetic, with J^* values about 20–50% higher than J [15–17]. But it must be realized that although these transitions are enhanced by the exchange mechanism with respect to the isolated MnF_6^{4-} center, there are no cases of their oscillator strengths ($\sim 10^{-4}$–10^{-3}) being as big as those measured for the 25000 cm^{-1} peak in $A_2MnCl_4 : Cu^{2+}$ (3×10^{-2}). Nevertheless, the present Mn–Cl–Cu coupled system is a special case since, at variance with fluorides, the $^4A_1\,{}^4E$ excitation of Mn^{2+} and the $Cl^-(eq) \rightarrow Cu^{2+}$ CT transition at 25000 cm^{-1} are resonant. Therefore, oscillator strength for Mn^{2+} excitations in Mn–Cl–Cu systems should be expected to be greater than in the corresponding Mn–F–Cu systems, provided that a chief mechanism for Mn^{2+} transitions to gain oscillator strength is the mixing

with CT states by configuration interaction in such exchange coupled systems.

Analogously, the in-plane polarized components of the $^4T_1$ and $^4T_2$ excitations of $MnCl_6^{4-}$ which are placed at 20000 and 21500 cm^{-1}, respectively, in both $(enH_2)MnCl_4$ [12] and A_2MnCl_4 [42], are nearly resonant with the $Cl^-(ax) \rightarrow Cu^{2+}$ CT transition. This CT band has been observed at 23150 cm^{-1} in the low temperature spectrum of $A_2CdCl_4 : Cu^{2+}$ (inset of Fig. 2 and Table 2) [13].

Therefore, we assign the two intense bands observed in $A_2MnCl_4 : Cu^{2+}$ and $A_2Cd_{0.7}Mn_{0.3}Cl_4 : Cu^{2+}$ to electronic transitions of Mn–Cu pairs from the ground state to excited states whose electronic wavefunctions involve both odd-symmetry $Cl^- \rightarrow Cu^{2+}$ CT states of the $CuCl_6^{4-}$ complex and Mn^{2+} spin–flip excitations. In particular, these mixed excited states correspond to the $Cl^-(eq) \rightarrow Cu^{2+}$ CT state and the $^4A_1{}^4E$ state of Mn^{2+} for the band at 25000 cm^{-1}, while for the band at 21000 cm^{-1}, the excited state involves the $Cl^-(ax) \rightarrow Cu^{2+}$ CT state and the in-plane polarized components of the $^4T_1$ and $^4T_2$ Mn^{2+} excitations. In this way, if we denote the excited states of the Mn–Cu pair by $|Mn^*Cu>$ and $|MnCu^*>$ (Mn^* means excited state of Mn^{2+}, and Cu^* corresponds to $Cl^- \rightarrow Cu^{2+}$ CT state), then the configurational interaction may lead to mixed states $\alpha|Mn^*Cu> + \beta|MnCu^*>$ and $\beta|Mn^*Cu> - \alpha|MnCu^*>$. The α and β coefficients will mainly depend on the matrix element $\langle MnCu^*|H_{ex}|Mn^*Cu>$ where H_{ex} is the hamiltonian relating the exchange interaction between these two excited pair states. Consequently, the oscillator strength of electric dipole (ED) transitions from the groun state $|MnCu>$ to either excited state of the pair is expected to be considerably greater than those for single $Cl^- \rightarrow Cu^{2+}$ CT transitions within an isolated $CuCl_6^{4-}$. This comes from the fact that the excited state wavefunctions of the pair spreads over the Mn–Cl–Cu cluster and therefore higher transition moments are likely. Hence these Mn chlorides doped with Cu^{2+} are outstanding systems to investigate exchange effects involving CT states.

The OA spectra of the mixed $A_2Cd_{1-x}Mn_xCl_4 : Cu^{2+}$ (Fig. 2) can be qualitatively explained within this scheme, taking into account that for $x = 0.3$, the presence of Mn–Cu dimers is predominant while only Mn–Cu–Mn trimers are formed for $x = 1$. Assuming that the Cd and Mn cations are randomly distributed among the metallic sites of the layer perovskite, the following aggregates will be formed in $A_2Cd_{0.7}Mn_{0.3}Cl_4 : Cu^{2+}$—19% of $CuCl_6^{4-}$ monomers; 66% of Mn–Cl–Cu dimers and 15% for Mn–Cl–Cu–Cl–Mn trimers. In this analysis only Mn–Cu–Mn systems forming bond angles of 180° are considered as trimers. On the other hand, the spectra of Fig. 2 clearly show that the bands at 25000 and 21000 cm^{-1} must be associated with distinct Mn–Cu exchange pathways since their relative intensity changes with the Mn concentration, x, according to the proposed assignment. The prominent intensity of the 25000 cm^{-1} band for $x = 0.3$ is explained within this figure assuming that the formation of Mn–Cu pairs connected through the equatorial Cu–Cl bond is more likely than those involving the axial Cu–Cl bond. The change of relative intensity observed from $x = 0.3$ to $x = 1$ would reflect an increase in the Mn–Cu(ax) with respect to the Mn–Cu(eq) since the same number of pairs are formed for $x = 1$. Although the effective ground state exchange constant, J, for Mn–Cu(ax) is expected to be much smaller than that for the Mn–Cu(eq) in Cu^{2+} complexes of D_{4h} symmetry due to the zero overlap between the b_{1g} (x^2-y^2) and the manganese wavefunction along the axial bond [15, 17], this is not true for the present systems where the real D_{2h} symmetry makes the unpaired mainly Cu^{2+} one-electron wavefunction to be: $\alpha|3z^2 - r^2> + \beta|x^2-y^2>$, that provides a non zero overlap between Cu and Mn along both the axial and equatorial bonds.

4.2.2. *Energy level diagram of* Mn–Cu *dimers and* Mn–Cu–Mn *trimers*. Figure 12 shows an approximate energy level diagram for a Mn–Cu dimer and a Mn–Cu–Mn trimer. We use an effective exchange hamiltonian of the type $H = 2J_{ex}\mathbf{S}_{Cu}.\mathbf{S}_{Mn}$ for both the ground and excited states, $J_{ex} = J$ and J^*, respectively. The Mn total spin is $S_{Mn} = 5/2$ for dimers and $\mathbf{S}_{Mn} = \mathbf{S}_{Mn1} + \mathbf{S}_{Mn2}$ ($S_{Mn} = 5, 4, 3, 2, 1, 0$) for trimers; $S_{Cu} = 1/2$ in all cases. It is important to point out that irrespective of the accuracy of this approximation to describe the exchange interaction between the excited states which can affect the energy of the sublevels, both the state description and the selection rules derived by this procedure are the same ones obtained through the actual exchange hamiltonians using the one electron spin operators:

$$H_{ex} = 2\sum_{ij} J_{ai\,bj}(\mathbf{s}_{Mn_i} \cdot \mathbf{s}_{Cu_j}) \qquad (3)$$

A D_{2h} symmetry is assumed for the Mn–Cu–Mn trimer according to the crystallographic structure of the host crystal. Thus the electronic ground state is described by the ket $|^6A_1(a)^2A_1{}^6A_1(b)>$ which transforms as $A_{1g} + B_{1u}$ in D_{2h}. The even (+) and odd (−) wavefunctions correspond to combination of the Mn^{2+} states $[^6A_1(a) \pm {}^6A_1(b)]/\sqrt{2}$. The unpaired Cu^{2+} wavefunction (mainly $d_{x^2-y^2}$) transform as a_{1g} in the local D_{2h} symmetry. The coupling of three spin $S_A = 5/2$, $S_B = 5/2$ and $S_{Cu} = 1/2$ gives rise to eleven spin states. The two Mn excited states $|^4A_1(a)^2A_1{}^6A_1(b)>$ and $|^6A_1(a)^2A_1{}^4A_1(b)>$ give rise

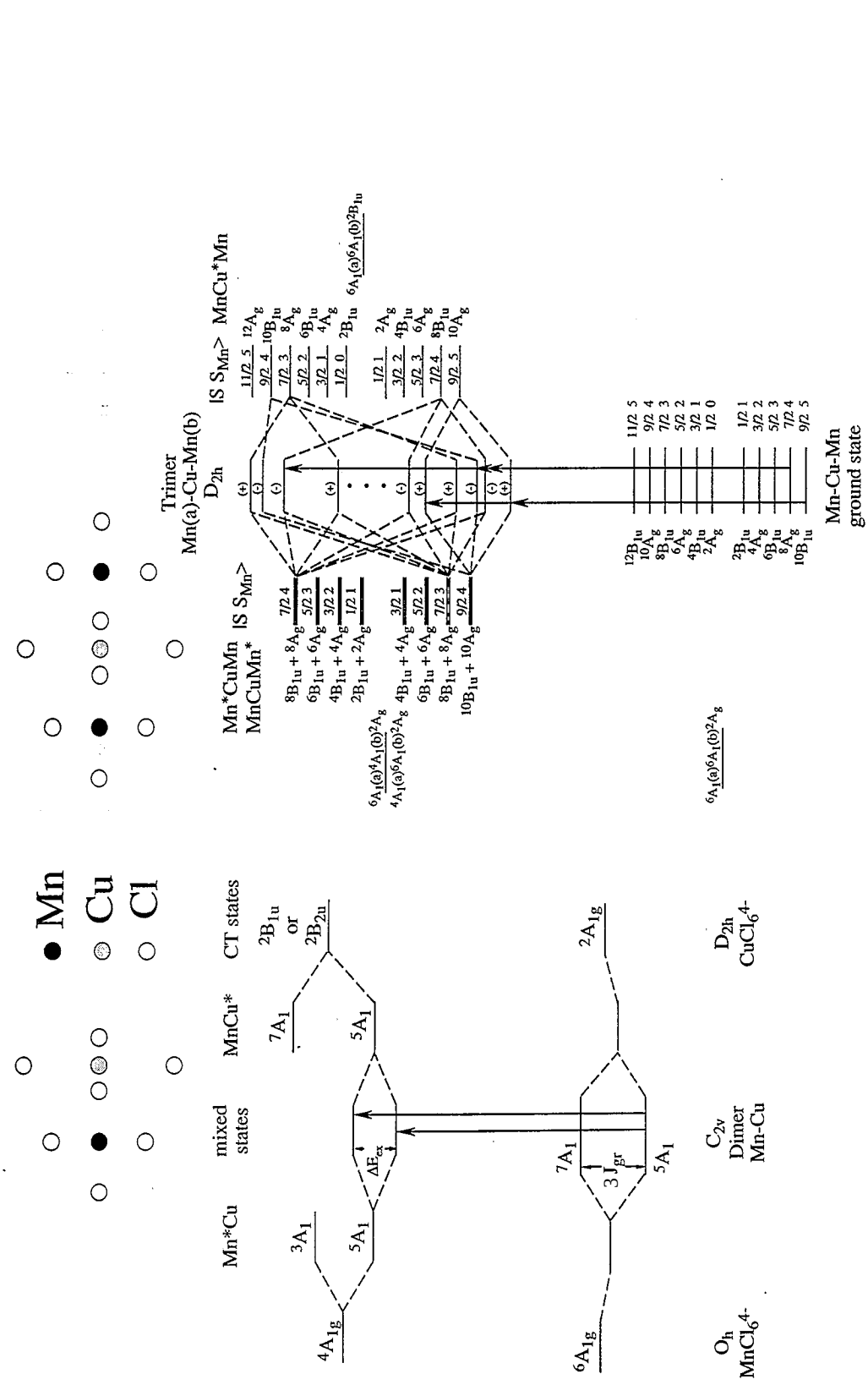

Fig. 12. Schematic energy level diagrams corresponding to a Mn–Cu dimer and a Mn–Cu–Mn trimer. The resonant $Cl^- \rightarrow Cu^{2+}$ charge transfer states have been included in each case. Arrows indicate the electric dipole transitions allowed by symmetry. In both cases, transitions are polarized along the Mn–Cu axis. For the sake of clarity, we only show the sublevels and electronic transitions corresponding to the highest spin values of the trimer. The (+) and (−) signs denote the even and odd parity of the sublevel, respectively.

to excited trimer states $^9B_{1g} + {}^9B_{1u}, \ldots$ (Fig. 12). These states are degenerate for the same spin value whenever the exchange interaction between these two states:

$$< {}^4A_1(a)^2A_1\,{}^6A_1(b)|H_{ex}|{}^6A_1(a)^2A_1\,{}^4A_1(b) >= 0$$

The exchange interaction between the $^2B_{1u}$ CT state of $CuCl_6^{4-}$ and the two Mn^{2+} ground state gives rise to a similar state diagram as for the ground state. These states also transform as $B_{1u} + A_{1g}$, but exchange the spin values. Given that the two excited states $|Mn^*Cu >$ and $|MnCu^* >$ are nearly resonant, they are mixed by configuration interaction provided that $< Mn^*Cu|H_{ex}|MnCu^* > \neq 0$. Within this scheme the only ED transitions allowed by symmetry correspond either to $A_{1g} \rightarrow B_{1u}$ or to $B_{1u} \rightarrow A_{1g}$ connecting states with the same spin value. These transitions are completely polarized along the Mn–Cu–Mn trimer axis.

Although the level diagrams shown in Fig. 12 foresee the existence of two and nineteen different allowed transitions for dimers and trimers, respectively, these are not resolved spectroscopically and therefore information about J^* cannot be directly extracted from the absorption spectra. However, proper values of the ground state exchange constant, J, can be obtained from the temperature dependence of the total oscillator strength, $f(T)$, provided that we know the relative intensity associated with each ground state sublevel of the trimer.

4.2.3. *Thermal dependence of the band intensity: influence of the* Mn–Cu *exchange interaction.* The shape of $f(T)$ allows us to distinguish between dimers and trimers since they exhibit rather different thermal behaviour. The variation of $f(T)$ for dimers and trimers are given respectively by the equations:

$$f(T) = \frac{f(0)}{\left[1 + \frac{7}{5}\exp(-3J/kT)\right]} \tag{4}$$

$$f(T) = 11 \times f(0)\left(\sum_i I_i \exp(-E_i/kT)\right)/Z \tag{5}$$

$Z = \sum_i g_i \exp(-E_i/kT)$ is the partition function of the trimer; I_i is the normalized relative intensity associated with the ith ground state sublevel; E_i and g_i are the corresponding energy and spin degeneracy, respectively; and $f(0)$ is the oscillator strength at $T = 0\,K$.

It is important to note that $f(T)$ can be exactly calculated for dimers given that only electronic transitions coming from the $^5A_1$ ground state sublevel are allowed. However, this is not the situation for trimers, where $f(T)$ depends on the different I_i values. Such values have been calculated by Mathonière *et al.* [18], for the $^6A_1 \rightarrow {}^4A_1$ spin–flip transition of Mn^{2+} in Mn–Cu–Mn trimers. According to the results in [18], the I_i relative intensity can be easily obtained on the basis of a spin-dependent transition moment operator, **P**, acting on exchange coupled Mn–Cu pairs [14, 43, 44]:

$$\mathbf{P} = \sum_{i=1}^{5} \mathbf{\Pi}_{Mn_iCu}(\mathbf{s}_{Mn_i} \cdot \mathbf{S}_{Cu}) \tag{6}$$

$$\mathbf{\Pi}_{Mn_iCu} = \mathbf{\Pi}_{Mn(a)_iCu} + \mathbf{\Pi}_{Mn(b)_iCu}$$

where $\Pi^j_{Mn_iCu} = \partial J_i/\partial E^j$ when $E^j \rightarrow 0$, $E^j (j = x, y, z)$ being the jth component of the light electric field. Symmetry considerations show that the x, y components of the $\mathbf{\Pi}_{Mn_iCu}$ vector are zero in a local C_{2v} pair symmetry (z is taken along the Mn–Cu line).

The relative intensity I_i is then given in terms of the 6-j symbols by:

$$I_i \propto | < S, S_{Mn}, S_{Cu}|\mathbf{P}|S, S^*_{Mnj}, S_{Cu} >|^2$$

and

$$\begin{aligned} &< S, S_{Mn}, S_{Cu}|\mathbf{P}|S, S^*_{Mnj}, S_{Cu} > \\ &\propto \sqrt{(2S_{Mn}+1)(2S^*_{Mn}+1)} \\ &\times \sqrt{3/2} \times \begin{Bmatrix} S^*_{Mn} & 1/2 & S \\ 1/2 & S_{Mn} & 1 \end{Bmatrix} \\ &\times \begin{Bmatrix} S_{Mn} & 1/2 & S^*_{Mn} \\ 3/2 & 5/2 & 5/2 \end{Bmatrix} \end{aligned} \tag{7}$$

The experimental variation of $f(T)$ for the two intense bands in $A_2MnCl_4 : Cu^{2+}$ (Fig. 11) are well explained within the trimer model using the I_i values calculated from eqn (7) [18]. Although these intensities do not necessarily correspond to our situation described in Fig. 12, since the moment operator of eqn (6) is valid only for spin–flip excitations without any change of orbital configuration, this result strongly suggests that a similar spin-dependent transition mechanism to that of eqn (6) must be involved in these trimer excitations. In no case can the variation of $f(T)$ for $A_2MnCl_4 : Cu^{2+}$ be described in terms of dimers, eqn (4).

It is important to realize that although the structural unit to describe the Mn–Cu interaction for $x = 1$ is an aggregate formed by one Cu and its four nearest Mn (pentamer), it can be shown (section 4.2.4) that the temperature dependence of the band intensity is that given by eqn (5). In fact, $f(T)$ has the same thermal dependence as a trimer if the spin- dependent transition moment operator for the two bands at 25000 and 21000 cm^{-1} involves Mn–Cu pathways along the axial and the equatorial Cu–Cl bonds, respectively.

Figure 11 shows the least-square fitting of $f(T)$ to eqn (5). The obtained ground exchange constants are $J(ax) = 65\,cm^{-1}$ for the 21000 cm^{-1} band and $J(eq) =$

$85\,cm^{-1}$ for the $25000\,cm^{-1}$ band. This difference between $J(ax)$ and $J(eq)$ confirms the distinct origin of these two bands and therefore justifies the present assignment.

It must be pointed out that $f(T)$ experiences an abrupt increase of about 5% at the SPT temperature, $T_{c1} = 92\,K$ (inset of Fig. 6). We associate this jump with an increase in the effective exchange constant induced by structural changes at T_{c1}. This SPT involves tilting of the inorganic MCl_6 octahedra which tends to bend the Mn–Cl–Mn bond, thus decreasing the exchange interaction below T_{c1}. In particular, this anomaly would reflect an increase $\Delta J = 2\,cm^{-1}$ provided that the z-component of the transition moment operator varies as the exchange constant, J. This STP has also an important influence on the transition energy of the band at $21000\,cm^{-1}$ where a redshift of $-350\,cm^{-1}$ is observed just above T_{c1} (Fig. 7). The fact that we do not observe a similar redshift in the $25000\,cm^{-1}$ band seems to confirm the assignment of these bands. Indeed those bands associated with the 10Dq-dependent $^4T_1$ and $^4T_2$ Mn^{2+} excitations are expected to be more sensitive than those associated with the 10Dq-independent $^4A_1$, ^4E excitations to changes of the local environment induced by SPT. Therefore these structural effects are important in distinguishing the origin of these bands.

The influence of SPTs upon the spectroscopic parameters is much stronger for the mixed $A_2Cd_{0.7}Mn_{0.3}Cl_4 : Cu^{2+}$ crystal. The anomalous behavior exhibited by $f(T)$ in the 80–150 K must be ascribed to structural effects induced by the SPT. At variance with the pure $A_2CdCl_4 : Cu^{2+}$ and $A_2MnCl_4 : Cu^{2+}$ crystals, the SPT around T_{c1} in the mixed crystal takes place in a broad temperature range probably due to the structural disorder and concentration gradients. This is evidenced by comparing the variation of $f(T)$ with those followed by the transition energy and the crystal absorbance at 700 nm (Figs 7 and 8). The latter variation reflects the critical scattering phenomena at the SPT temperature which extends over a wide temperature range $\Delta T = 70\,K$ in $A_2Cd_{0.7}Mn_{0.3}Cl_4 : Cu^{2+}$. This fact together with the different type of Mn–Cu aggregates formed in this mixed crystal makes it difficult to perform a precise analysis of the variation of $f(T)$. However, we can roughly explain this variation in terms of dimers. Such an analysis has been done outside the 80–150 K range to avoid the SPT effects. Figure 11 shows the calculated $f(T)$ curves from eqn (4) below 80 K and above 150 K. We obtain exchange constants of 65 and $70\,cm^{-1}$, respectively. The increase of $f(T)$ from 80 to 150 K is probably associated with a continuous increase of the effective exchange constant, $J(T)$, as well as of the transition moment parameter, $\Pi^z(T)$, due to reorientational motions of the MCl_6 octahedra induced by the SPT. The increase of the exchange constant, $\Delta J = 5\,cm^{-1}$, and the analogous increase experienced by the extrapolated oscillator strength at $T = 0\,K$, $\Delta f(0) = 0.01$ in the same temperature range, can be accounted for if we assume that, like for trimers, the z-component of the transition moment operator, Π^z, varies as the exchange constant J.

4.2.4. *Variation of $I(T)$ in $A_2MnCl_4 : Cu^{2+}$—a Mn_4–Cu pentamer model.* Let us consider the pentamer formed by one Cu^{2+} and the four Mn neighbors in $A_2MnCl_4 : Cu^{2+}$. Two Mn are along the axial Cu–Cl direction and the other Mn are along the equatorial Cu–Cl one. We only consider the four nearest Mn^{2+} ions around the Cu^{2+} impurity for describing the aggregate given that the antiferromagnetic Mn–Mn exchange interaction of the bulk, $J = 5\,cm^{-1}$ [45], is much weaker than the corresponding Mn–Cu exchange constant ($J = 65\,cm^{-1}$).

Within this model it can be shown that the variation of the band intensity with temperature is that of eqn (5), provided that the corresponding transition moment associated with the electronic transition involves either the axial or the equatorial pathway.

The exchange hamiltonian of a pentamer is given by:

$$H_{ex} = J(ax)\mathbf{S}^{ax}_{Mn} \cdot \mathbf{S}_{Cu} + J(eq)\mathbf{S}^{eq}_{Mn} \cdot \mathbf{S}_{Cu} \qquad (8)$$

where $\mathbf{S}^{eq}_{Mn} = \mathbf{S}^1_{Mn} + \mathbf{S}^2_{Mn}$ and $\mathbf{S}^{ax}_{Mn} = \mathbf{S}^3_{Mn} + \mathbf{S}^4_{Mn}$. Manganese 1, 2 and 3, 4 are along the axial and equatorial Cu–Cl bonds, respectively. Denoting by $|S^{eq}, S^{eq}_{Mn}, S^{ax}, S^{ax}_{Mn}, S_{Cu}>$ the states of the pentamer, the dipole moment matrix element related to the axial exchange pathway is:

$$\begin{aligned} &< S^{eq}, S^{eq}_{Mn}, S^{ax}, S^{ax}_{Mn}, S_{Cu}|\mathbf{P}_{ax}|S^{eq'}, S^{eq'}_{Mn}, S^{ax'}, S^{ax'}_{Mn}, S_{Cu} > \\ &= \delta_{S^{eq},S^{eq'}} \times \delta_{S^{eq}_{Mn},S^{eq'}_{Mn}} \times \delta_{S^{ax},S^{ax'}} \\ &\quad < S^{ax}, S^{ax}_{Mn}, S_{Cu}|\mathbf{P}_{ax}|S^{ax}, S^{ax'}_{Mn}, S_{Cu} > \end{aligned} \qquad (9)$$

This matrix element is equal to that given in eqn (7) for a trimer. The energy of each ground state sublevel is

$$\begin{aligned} E &= E_{ax_i} + E_{eq_j} \\ &= \frac{J(ax)}{2}[S^{ax}(S^{ax}+1) - S^{ax}_{Mn}(S^{ax}_{Mn}+1) \\ &\quad - S_{Cu}(S_{Cu}+1)] + \frac{J(eq)}{2}[S^{eq}(S^{eq}+1) \\ &\quad - S^{eq}_{Mn}(S^{eq}_{Mn}+1)S^{eq}_{Mn} - S_{Cu}(S_{Cu}+1)] \end{aligned} \qquad (10)$$

Therefore, the temperature dependence of the total relative intensity of a band involving the axial

transition moment operator, $\mathbf{P}_{ax}$, is:

$$I^{ax}(T) = \frac{\sum_{ij} I_i g_j e^{-(E_{ax_i}+E_{eq_j})/kT}}{Z} = \frac{\left(\sum_i I_i e^{-E_{ax_i}/kT}\right)\left(\sum_j g_j e^{-E_{eq_j}/kT}\right)}{Z} \quad (11)$$

$$Z = \left(\sum_i g_i e^{-E_{ax_i}/kT}\right)\left(\sum_j g_j e^{-E_{eq_j}/kT}\right)$$

where the i, j subscripts include all the axial and equatorial *trimer* sublevels. A similar equation is obtained for $I^{eq}(T)$ when the equatorial transition operator $\mathbf{P}_{eq}$ is employed. Note that eqns (5) and (11) provide the same intensity thermal dependence, $I(T)$.

5. CONCLUSIONS

The main feature of the present work is the strong influence of Mn^{2+} on the optical properties of Cu^{2+} doped $A_2Cd_{1-x}Mn_xCl_4$ crystals. Although the local structure around the Cu^{2+} is almost the same along the series, an important intensity enhancement of the $Cl^- \rightarrow Cu^{2+}$ CT bands induced by the exchange interactions with the nearest Mn^{2+} neighbors is observed. At variance with other Mn–Cu coupled systems formed in fluorides, the present systems are very attractive in the investigation of exchange effects, given that the $Cl^- \rightarrow Cu^{2+}$ CT states are nearly resonant with some Mn^{2+} excited states. This renders the excited state associated with the optical excitation highly delocalized along the Mn–Cl–Cu path and therefore greater transition moments are likely.

It is worth pointing out that these effects have not been found in other Mn chlorides doped with Cu^{2+} whose Mn–Cl–Cu pathway angle deviates from 180°. The 1D $[(CH_3)_4N]MnCl_3 : Cu^{2+}$ is an example of this behavior. The synthesis of new compounds containing exchange coupled Mn–Cl–Cu systems with different structural geometries would be highly desirable in order to clarify the influence of the exchange pathway upon the optical spectra.

Acknowledgements—We thank Professor H. U. Güdel, Prof. M. A. Hitchman, and Prof. M. Moreno for helpful discussions and information. The collaboration of B. Baticle in this work is kindly acknowledged. This investigation has been supported by Caja Cantabria and the CICYT (Project No. PB-0505).

REFERENCES

1. Lever A. B. P., *Inorganic Electronic Spectroscopy*, 2nd Ed., Elsevier, Amsterdam (1984).
2. Reinen D. and Atanasov M., *Magnetic Resonance Review* **15,** 167 (1991).
3. Hitchman M. A., *Comm. Inorg. Chem.* **15,** 197 (1994).
4. Finnie K., Dubicki L., Krausz E. R. and Riley M. J., *Inorg. Chem.* **29,** 3908 (1990).
5. Reinen D., Steffen G., Hitchman M. A., Stratemeier H., Dubicki L., Krausz E. R., Riley M. J., Mathies H. E., Recker K. and Wallrafen F., *Chem. Phys.* **155,** 117 (1991).
6. Riley M. J., Hitchman M. A. and Reinen D., *Chem. Phys.* **102,** 11 (1986).
7. Riley M. J., Dubicki L., Moran G., Krausz E. R. and Yamada I., *Chem. Phys.* **145,** 363 (1990).
8. Halvorson K. E., Patterson C. and Willett R. D., *Acta Cryst. B* **46,** 508 (1990).
9. Bloomquist D. R., Pressprich M. R. and Willet R. D., *J. Am. Chem. Soc.* **110,** 7391 (1988).
10. Moral B. A. and Rodríguez F., *Rev. Sci. Inst.* **66,** 5178 (1995).
11. Aramburu J. A. and Moreno M., *J. Chimie Physique* **86,** 871 (1989).
12. Schmid U., Güdel H. U. and Willet R. D., *Inorg. Chem.* **21,** 2977 (1982).
13. Baticle B., Rodríguez F. and Valiente R., *Radiation Effects and Defects in Solids* (in press).
14. Ferguson J., Guggenheim H. J. and Tanabe Y., *J. Phys. Soc. Jpn.* **21,** 692 (1966).
15. Ferguson J., Guggenheim H. J. and Krausz E. R., *J. Phys. C: Solid State Phys.* **4,** 1866 (1971).
16. Ferguson J. and Guggenheim H. J., *Phys. Rev. B* **1,** 4223 (1970).
17. Ferré J. and Régis M., *Sol. State Commun.* **26,** 225 (1978).
18. Mathonière C. and Kahn O., *Inorg. Chem.* **33,** 2103 (1994).
19. Mathonière C., Kahn O., Daran J. C., Hilbig H. and Köhler F. H., *Inorg. Chem.* **32,** 4057 (1993).
20. Rodríguez-Carvajal J., *Abstract of the Satellite Meeting on Powder Diffraction of the XV Congress of the International Union of Crystallography*, Toulouse, France, p. 127 (1990).
21. Fowler W. B., *Physics of Color Centers*, p. 72. Academic Press, New York (1968).
22. Arend H., Hofmann R. and Waldner F., *Sol. State Commun.* **13,** 1629 (1973).
23. Knorr K., Jahn I. R. and Heger G., *Sol. State Commun.* **15,** 231 (1974).
24. Heger G., Mullen D. and Knorr K., *Phys. Stat. Sol(a)* **35,** 627 (1976).
25. Depmeier W., Felsche J. and Wildermuth G., *J. Sol. State Chem.* **21,** 57 (1977).
26. Valiente R., Marco de Lucas M. C. and Rodríguez F., *J. Phys.: Condens. Matter* **6,** 4527 (1994).
27. Chapuis G., Arend H. and Kind R., *Phys. Stat. Sol.* **31,** 449 (1975).
28. Lehner N., Strobel K., Geik R. and Heger G., *J. Phys. C: Solid State Phys.* **8,** 4096 (1978).
29. Desjardins S. R., Penfield K. W., Cohen S. L., Musselman R. L. and Solomon E. I., *J. Am. Chem. Soc.* **105,** 4590 (1983).
30. Tichy K., Beues J., Hälg W. and Arend H., *Acta Cryst. B* **34,** 2970 (1978).
31. Kan'no K., Naoe S., Mukai S. and Nakai Y., *Solid State Commun.* **13,** 1325 (1973).
32. Kan'no K., Mukai S. and Nakai Y., *J. Phys. Soc. Jpn* **36,** 1492 (1974).
33. McDonald R. G. and Hitchman M. A., *Inorg. Chem.* **28,** 3996 (1989).
34. Rodríguez F., Nuñez P. and Marco de Lucas M. C., *J. Sol. State Chem.* **110,** 370 (1994).
35. Aramburu J. A. and Moreno M., *J. Chem. Phys.* **83,** 6071 (1985).
36. Agulló-López F., Calleja J. M., Cussó F., Jaque F. and López F. J., *Prog. Mater. Sci.* **39,** 187 (1986).
37. Marco de Lucas M. C., Rodríguez F. and Moreno M., *Phys. Stat. Sol. (b)* **184,** 247 (1994).

38. McCarthy P. and Güdel H. U., *Inorg. Chem.* **25,** 838 (1986).
39. Kind R., *Phys. Stat. Sol.* **44,** 661 (1977).
40. Windsor C. G. and Stevenson R. W. H. *Proc. Phys. Soc.* **87,** 501 (1966).
41. Yamada I., *J. Phys. Soc. Jpn.* **33,** 979 (1972).
42. Morita M. and Kameyama M., *J. Lumin.* **24/25,** 79 (1981).
43. Ferguson J., Guggenheim H. J. and Tanabe Y., *Phys. Rev.* **161,** 207 (1967).
44. Güdel H. U., *Magneto-Structural Correlations in Exchange Couple Systems* (Edited by R. D. Willet, D. Gatteschi and O. Kahn), Vol. 140, p. 297. D. Reidel, Dordrecht (1985).
45. Van Amstel W. D. and de Jongh L. J., *Sol. State Commun.* **11,** 1423 (1972).
46. Nelson H. C., Simonsen S. H. and Watt G. W., *J. Chem. Soc. Chem. Commun.* 632 (1979).
47. Riley M. J. and Hitchman M. A., *Inorg. Chem.* **28,** 3996 (1989).
48. McDonald R. G. and Hitchman M. A., *Inorg. Chem.* **25,** 3273 (1987).
49. Harlow R. L., Wells W. J., Watt G. W. and Simonsen S. H., *Inorg. Chem.* **13,** 2106 (1974).
50. Hitchman M. A. and Cassidy P., *Inorg. Chem.* **18,** 1745 (1979).
51. Cassidy P. and Hitchman M. A., *J. Chem. Soc. Chem. Commun.* 837 (1975).
52. Udupa M. R. and Krebs B., *Inorg. Chim. Acta* **33,** 241 (1979).
53. Suetler A. W., Jacobseon R. A. and Rundle R. E., *Inorg. Chem.* **28,** 3996 (1966).
54. Laiho R., Natarajan M. and Kaira M., *Phys. status solidi A* **15,** 311 (1973).
55. Steadman J. P. and Willet R. D., *Inorg. Chim. Acta* **4,** 367 (1970).
56. Hitchman M. A. and Cassidy P., *Inorg. Chem.* **17,** 1682 (1978).
57. Barendgret F. and Schemk H., *Physica* **49,** 465 (1970).
58. Morosin B., Fallon P. and Valentine J. S., *Acta Cryst. B* **31,** 2220 (1975).
59. Hatfield W. E. and Piper T. S., *Inorg. Chem.* **3,** 841 (1964).